JCTC Journal of Chemical Theory and Computation

Hydrogen Interaction in Ti-Doped $LiBH_4$ for Hydrogen Storage: A Density Functional Analysis

Jianjun Liu and Qingfeng Ge*

Department of Chemistry and Biochemistry, Southern Illinois University, Carbondale, Illinois 62901

Received June 4, 2009

Abstract: Density functional theory studies have been carried out to investigate the energetics and structures of Ti-doped $LiBH_4$ (001), (100), and (010) surfaces. The possibilities of Ti occupying various positions at these surfaces leading to substitution, surface adsorption, and interstitial insertion are examined. Among all possible structures, a Ti atom energetically prefers to occupy interstitial positions involving three or four BH_4^- hydrides and to stay above the top layer of B atoms. The most stable species on the three surfaces have a similar local structure, described as $TiB_2H_8-nBH_4$ ($n = 1, 2$), with varying spin states. Molecular orbital analysis for the local structures showed that the structural stability could be attributed to the symmetry-adapted orbital overlap between Ti and "inside" B−H bonds. Furthermore, the hydrogen desorption energies from many positions in these local complex structures were reduced significantly with respect to that from the clean surface. The most favorable hydrogen desorption pathways are found to lead to triplet dehydrogenation products. Therefore, the triplet $TiB_2H_8-BH_4$ in (001) and $TiB_2H_8-2BH_4$ in (010) can desorb hydrogen in molecular form, while the quintet $TiB_2H_8-BH_4$ in (100) must first desorb hydrogen atoms, followed by the formation of a hydrogen molecule in the gas phase. The catalytic effect of Ti doped in $LiBH_4$ has been compared with that in $NaAlH_4$.

1. Introduction

Many attempts have been made to develop new materials with high hydrogen storage capacities in order to meet the demand of commercial vehicles powered by H_2/O_2 proton exchange membrane fuel cells.[1−3] Lithium borohydride ($LiBH_4$) has been an attractive candidate due to its intrinsically high gravimetric and volumetric hydrogen capacities (18.2 wt %, 121 kg/m^3).[2] Unfortunately, pure $LiBH_4$ material is too stable and only liberates 2% of the hydrogen even at the melting point (541−559 K).[4] For $LiBH_4$, the partial decomposition to $LiH(s) + B(s) + 3/2H_2(g)$ has a standard enthalpy of 100.3 kJ/mol.[5] The highly endothermic reaction indicates that dehydrogenation of $LiBH_4$ must be performed at elevated temperatures. The experimental results of Züttel et. al showed that a significant hydrogen desorption peak started at 673 K and reached its maximum value around 773 K.[6] In order to use $LiBH_4$ as a practical hydrogen storage material, the enthalpy of the dehydrogenation reaction has to be reduced, by either stabilizing the dehydrogenated state or destabilizing the hydrogenated state.

Many compounds which bind strongly to borohydrides or provide a source to allow partial substitution of Li cations have been mixed with $LiBH_4$. Züttel et al. found that 75% $LiBH_4$ mixed with 25% SiO_2 can reduce the initial hydrogen release temperature from 673 to 523 K.[6] On the other hand, the rehydrogenation reaction will not occur under mild conditions. The same authors reported that synthesizing $LiBH_4$ from its elements under conditions up to 923 K and 150 bar of H_2 pressure was unsuccessful.[6] Mixing compounds with cations of similar size to Li but having a higher valence, such as Mg^{2+}, was also attempted.[7] The temperature of the dehydrogenation reaction was lowered by approximately 30 K when Li in $LiBH_4$ was partially substituted by Mg^{2+}. Vajo et al. reported a more complicated mixture of $LiBH_4$ and $LiH + 0.5MgB_2$, doped with 2−3 mol % $TiCl_3$. They showed that 9 wt % hydrogen was adsorbed at 627 K

* Corresponding author e-mail: qge@chem.siu.edu.

10.1021/ct900287r CCC: $40.75
Published on Web 10/01/2009

and 100 bar, neglecting the weight of $TiCl_3$.[8] Their P−C−T isotherms demonstrated that the addition of MgH_2 reduced the rehydrogenation/dehydrogenation enthalpy by ∼25 kJ/(mol H_2) compared with the pure $LiBH_4$ material. A finding relevant to the present study is that their initial experiments without $TiCl_3$ displayed poor kinetic performance. Recently, Au et al. showed that $LiBH_4$ modified by metal oxides or metal chlorides, such as TiO_2 and $TiCl_3$, could reduce the dehydrogenation temperature and achieve rehydrogenation under moderate conditions.[9,10] Modified $LiBH_4$ releases 9 wt % H_2, starting as low as 473 K, which is significantly lower than the hydrogen-releasing temperature of 673 K for pure $LiBH_4$. After being dehydrogenated, the modified $LiBH_4$ can absorb 7−9 wt % H_2 at 873 K and 70 bar, a significant improvement from 923 K and 150 bar for pure $LiBH_4$. Very recently, Fang et al. reported that a mechanically milled $3LiBH_4/TiF_3$ mixture released 5−6 wt % hydrogen at temperatures of 343−363 K.[11] Similarly, the use of other dopants has been attempted to reduce the hydrogen desorption temperature of MgH_2.[12,13] Clearly, the addition of Ti compounds (TiO_2, $TiCl_3$, and TiF_3) results in a strong improvement for hydrogen desorption and, to a lesser extent, for rehydrogenation. On the other hand, the improvement brought by these additives to $LiBH_4$ is not sufficient to make $LiBH_4$ viable as a practical hydrogen storage medium in spite of its structural similarity to $NaAlH_4$. Chemically, boron holds onto its hydrogen atoms tighter in $LiBH_4$ than aluminum does in $NaAlH_4$. A comparative study of Ti-doped $LiBH_4$ and $NaAlH_4$ would provide some insights into the effect of doped Ti on hydrogen interactions in these materials. Previously, we identified an interstitial $TiAl_3H_{12}$ complex structure to be the most stable species in both Ti-doped $NaAlH_4$(001) and (100) surfaces.[14,15] Hydrogen desorption energies from many positions of the $TiAl_3H_{12}$ complex structure were reduced considerably as compared with that from an undoped surface. Our prediction of the complex structure was confirmed subsequently by an experimental study: the interstitial structure was shown to account for 75% of all Ti doped in $NaAlH_4$.[16] Furthermore, we studied 3d-transition-metal (TM)-doped $NaAlH_4$(001) and found that the stability of $TMAl_3H_{12}$ and its desorption energies correlate with the 18-electron rule.[17] The coordination chemistry of a transition metal with tetrahydroborate ligands has been extensively discussed in the literature.[18−23] The electron-counting rule and electronic structure analysis were used to explain the stability of molecular complexes such as $Ti(BH_4)_3$.[18,20,23,24] Considering that $Ti(BH_4)_n$ may be formed in Ti-doped $LiBH_4$, it is expected that the explanation and analysis applied in $Ti(BH_4)_3$ can be helpful in understanding the stability of local structures in Ti-doped $LiBH_4$. On the other hand, we expect some discrepancies between $Ti(BH_4)_n$ in Ti-doped $LiBH_4$ and the complex $Ti(BH_4)_3$ because of the different ligand charge. Furthermore, electron redistribution in a saltlike solid-state complex may cause the electron-counting rule to be different from that of the isolated clusters. The creation of the surface will further change the local environment of the ions, especially in regions close to the surface.

Herein, we explored the effect of added Ti to the B−H interaction in $LiBH_4$ on the basis of various surface models. We examined the structures and the stabilities of $LiBH_4$ (001), (100), and (010) surfaces doped with a Ti atom. On the basis of the most stable structures, we computed the hydrogen desorption energies and compared them with those of undoped $LiBH_4$ surfaces. We also compared the effect of doped Ti in $LiBH_4$ surfaces with that in $NaAlH_4$ surfaces and identified key differences between the two systems.

2. Computational Details

Periodic density functional theory (DFT) calculations with spin-polarization were carried out using the VASP code.[25,26] The electron−ion interactions were described by the projector augmented wave (PAW).[27] The valence electrons of Li $2s^12p^0$, B $2s^22p^1$, H $1s^1$, and Ti $3d^34s^1$ were treated explicitly with a plane-wave basis set at a cutoff energy of 400 eV. The exchange-correlation energy was calculated with the PBE form of the generalized gradient-corrected functional.[28,29] The surface Brillouin zone was sampled with the K points generated by the Monkhorst−Pack scheme and with a space less than 0.05 $Å^{-1}$.[30] Similar parameters have been used in our previous calculations, in which test results were consistent with experimental observation.[14,15,17,31,32]

The supercell structures of clean $LiBH_4$ surfaces were built from the optimized bulk structure.[32] The vacuum spaces in all surface calculations are larger than 15 Å along the z direction. The geometries of slabs were optimized by the quasi-Newton or conjugate-gradient method as implemented in VASP. A Gaussian electronic smearing of 0.1 eV was employed to improve the convergence of electronic self-consistent cycles. The convergence criteria for energy and force are 1.0×10^{-6} eV and 0.05 eV/Å, respectively. Six layers of B atoms were included in the slabs, simulating the surfaces. The Li and B atoms in the bottom two layers of the slab were fixed at their corresponding bulk positions, while the Li and B atoms in the top four layers as well as all of the hydrogen atoms were allowed to relax according to the Hellman-Feynman forces. The total energies of the relaxed slabs were used as references to calculate the binding energy for Ti doped in different positions. The reference energy of the Ti atom was calculated by placing a Ti atom in a large box with spin-polarization. The converged self-consistent field cycles resulted in a Ti atom with a quintet multiplicity, consistent with the electronic ground state of the Ti atom.[33] The electronic structures of local structures were calculated using Gaussian03 without further optimization and analyzed with GaussView 3.0.[34] The atomic electronic charges were determined according to the Bader's scheme implemented by Henkelman and Jonsson.[35]

3. Results and Discussion

3.1. Energetics and Structures of Ti-Doped $LiBH_4$. A number of experimental studies of $TiCl_3$-doped sodium alanates indicated that Ti was reduced to zero valence and dispersed into the host materials.[36−42] We therefore chose to study the Ti atom interaction with the $LiBH_4$ surfaces. The slabs of three clean surfaces, that is, (001), (100), and

(010), were optimized first. The unit cells of these surfaces have lateral dimensions of 7.1065 × 8.6532, 8.6532 × 6.6140, and 6.6140 × 7.1065 Å^2, respectively.[32] The clean (100) and (010) surfaces have a surface energy of ∼0.12 J/m^2 and are significantly more stable than the (001) surface.[32] On the basis of the relaxed clean surfaces, several possible positions for adding Ti in the $LiBH_4$ surfaces were considered. The relaxed structures are shown in Figure 1a, the (001) surface, 1b, the (100) surface, and 1c, the (010) surface. The binding energy and Bader charge of Ti are also given in each structure. In all of the structures, Ti loses electrons and becomes positively charged. Furthermore, the Bader charge on Ti depends on its depth/position and coordination with the BH_4^- units. According to the final position of the Ti atom, the relaxed structures were classified as interstitial insertion, surface adsorption, and substitution of Li, which were prefixed with *Inter*, *Surf*, and *Sub*, respectively. We note that *Surf* corresponds to the structures in which Ti interacts with BH_4^- through H only. In order to account for the local geometric structures, we categorized the arrangements of the BH_4^- ligands around the Ti atom into T-shape, linear, triangle, and square. The binding energies, the depth of the Ti atom with respect to the surface layer B atoms, as well as the local geometric shape are all summarized in Table 1.

For Ti-doped $LiBH_4$ (001) surface, *Inter_1*, with a binding energy of −2.598 eV, is energetically the most stable among all relaxed structures of the Ti-doped $LiBH_4$ (001) surface. In *Inter_1*, Ti connects with two BH_4^- units in the first layer via Ti−B and Ti−H bonds and interacts with a third BH_4^- unit in the second layer through a Ti−H bond, as shown in Figure 1a. The local structure of *Inter_1* is referred to as $TiB_2H_8-BH_4$, distinguishing the BH_4^- unit in the second layer from those in the top layer. The Ti atom and three BH_4^- ligands form a T-shape geometric arrangement. *Inter_5*, which has a similar local structure to *Inter_1*, is 1.374 eV less stable. The obvious difference between *Inter_5* and *Inter_1* is the location of the Ti in the former with respect to the surface: Ti is situated 4.387 Å below the first layer B atoms in *Inter_5*, whereas the Ti depth is only 0.343 Å in *Inter_1*. In fact, there is a correlation between the depth of Ti in the slab and the stability of the structure for the same type of doping mode (interstitial insertion, surface absorption, and substitution) in the same surface.

The slab representing the $LiBH_4$ (100) surface has a double-layered arrangement, that is, the layer spacing alternates between large and small. This resulted in two possible slab models for the surface: one with an arrangement of a small interlayer spacing between the top and second layers and a large one between the second and the third layers and another with the reversed arrangement. Our results show that the first one is 0.121 eV more stable than the second. Therefore, we chose the first arrangement as our model for the (100) surface.

Doped Ti interacts primarily with the BH_4^- units in the first two layers. Again, *Inter_1* is the most stable structure among all of the relaxed structures of the Ti-doped $LiBH_4$ (100) surface and has a binding energy of −1.608 eV. Three surrounding BH_4^- units and the Ti atom form a T-shape local arrangement. We note that the local structure of *Inter_1* in the (100) surface is very similar to that of *Inter_1* in the (001) surface and can also be denoted as $TiB_2H_8-BH_4$. As shown in Figure 1b, the substitutional doping (*Sub_1* and *Sub_2*) seems to result in local structures similar to those in interstitial insertion. However, these structures are much less stable. The reduced stabilities of these structures are related to the displacement of Li cations, which costs a significant amount of energy. The weaker electron-donating ability of Ti relative to that of Li causes fewer electrons to be donated from Ti to the sp^3 orbitals of BH_4^-, leading to an incomplete occupancy of the bonding orbitals.

The results of doping Ti in the $LiBH_4$ (010) surface are similar; that is, the interstitial insertion is energetically the most favorable doping mode. In *Inter_1* formed on the (010) surface, two BH_4^- units in the second layer share their interactions with the two BH_4^- units in the top layer, forming a $TiB_2H_8-2BH_4$ local complex. The binding energy of this structure is −1.709 eV. Geometrically, $TiB_2H_8-2BH_4$ forms a square arrangement.

In summary, doped Ti prefers the interstitial position formed by three or four BH_4^- units, forming a $TiB_2H_8-BH_4$ complex in the (001) and (100) surfaces and a $TiB_2H_8-2BH_4$ complex in (010). In the most stable structures, Ti sits in the first layer of the $LiBH_4$ surface. The detailed local structures are replotted in Figure 2 by removing other Li atoms and other BH_4^- units that are not directly connected to the Ti atom. The atoms in those structures are numbered in Figure 2 and will be referred to as such in the following sections. Although $TiB_2H_8-BH_4$ (T-shape) and $TiB_2H_8-2BH_4$ (square) have different geometric arrangements, the main part of the structures, TiB_2H_8, is very similar in the three structures. In fact, the linear TiB_2H_8 is the main constituent of the structure and determines the stability of the structures. This analysis is supported by the fact that the binding energies of *Inter_1* and *Inter_2* in the Ti-doped $LiBH_4$ (001) surface only differ by 0.189 eV. However, these binding energies are much smaller than that of Ti in the $TiAl_3H_{12}$ structure formed upon doping Ti in $NaAlH_4$ (−4.182 eV).[14] We showed that doping Ti in $NaAlH_4$ would become thermodynamically unfavorable if bulk Ti was used as a reference state.[17] Doping Ti in $LiBH_4$ will be more endothermic than in $NaAlH_4$.

3.2. Hydrogen Desorption from $TiB_2H_8-BH_4$ and $TiB_2H_8-2BH_4$. Many experiments showed that the Ti-containing compounds in alanate-based materials enhanced the dehydrogenation kinetics and improved the rehydrogenation conditions.[16,37,40,43−46] We attributed the reduction in dehydrogenation temperatures to the formation of the $TiAl_3H_{12}$ complex. We showed that hydrogen desorption energies from many positions of the complex were reduced compared to the undoped surfaces. Furthermore, our analyses indicated that the effect was not localized to the complex structure. Herein, we examined the effect of doped Ti in $LiBH_4$ on dehydrogenation on the basis of the most stable structures: $TiB_2H_8-BH_4$ on (001) and (100) and $TiB_2H_8-2BH_4$ on (010).

We note that the most stable structures carry net magnetic moments. Our further analyses of local spin-density showed

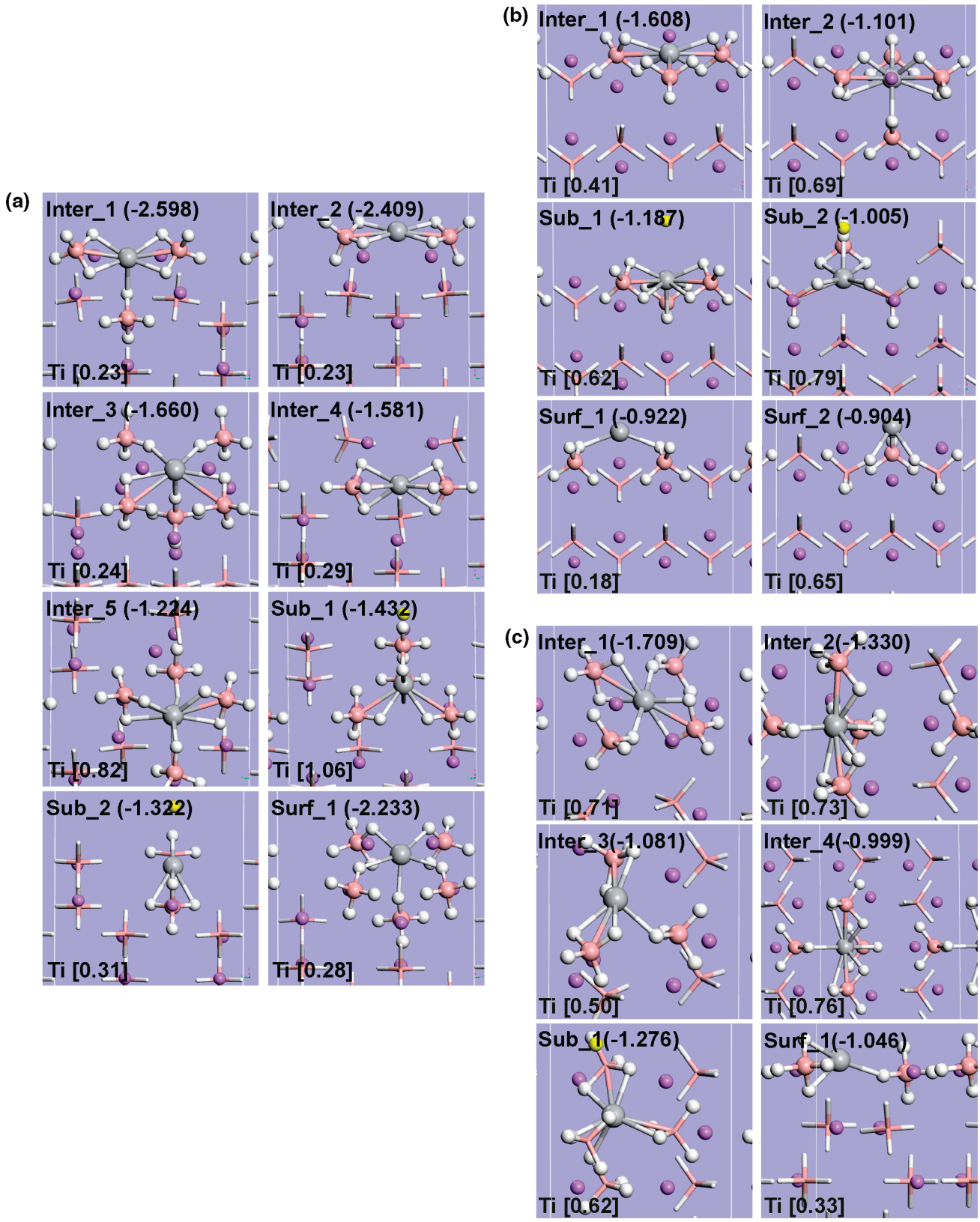

Figure 1. The DFT-GGA relaxed structures of Ti doped in the (a) (001), (b) (100), and (c) (010) surface of $LiBH_4$. The binding energy and net Bader charge of Ti are given in the top-left and bottom-left corners of each structure, respectively. The white, peach, purple, and gray balls represent H, B, Li, and Ti atoms, respectively. The yellow ball in the substitution structures represents the Li atom substituted by the Ti atom.

that the magnetic moments were largely localized to Ti, with some residual spins (1 to 2 orders of magnitude lower than on Ti) on the neighboring BH_4^- units but limited to the $TiB_2H_8{-}nBH_4$ (n = 1, 2) local structures. The resulting magnetic moments are integers in most cases. Even in the few cases of noninteger values, they are within 0.01 from the closest integer. Therefore, we borrowed the terms that have been used to describe isolated molecules and considered

Table 1. Binding Energies, Depth of Ti with Respect to the First Layer of B, and Shape of Local Structures in the Ti-Doped $LiBH_4$ (001), (100), and (010) Surfaces

			binding energy (eV)		
species	depth	ligand	singlet	triplet	quintet
		Ti-Doped $LiBH_4$ (001)			
Inter_1	−0.343	T-shaped	−2.256	−2.598	−2.580
Inter_2	+0.233	linear	−2.181	−2.409	−2.205
Inter_3	−0.743	square	−1.475	−1.660	−1.716
Inter_4	−2.048	linear	−1.261	−1.442	−1.581
Inter_5	−4.387	T-shaped	−1.154	−1.224	−1.205
Sub_1	−2.053	triangle		−1.432	−1.422
Sub_2	−0.445	linear	−1.048	−1.315	−1.322
Surf_1	−0.547	square		−2.132	−2.233
		Ti-Doped $LiBH_4$ (100)			
Inter_1	−0.059	T-shaped	−1.010	−1.392	−1.608
Inter_2	−0.937	T-shaped	−0.598	−0.870	−1.101
Sub_1	−0.095	T-shaped	−0.987	−1.187	−0.834
Sub_2	−1.233	triangle	−0.873	−1.005	−0.881
Surf_1	+1.148	linear	−0.213	−0.922	−0.790
Surf_2	+1.233	triangle	−0.242	−0.481	−0.904
		Ti-Doped $LiBH_4$ (010)			
Inter_1	−0.907	square	−1.594	−1.709	−1.444
Inter_2	−2.399	T-shape	−1.093	−1.330	−1.270
Inter_3	−0.699	triangle	−0.670	−0.924	−1.081
Inter_4	−4.431	T-shape	−0.779	−0.999	−0.408
Sub_1	−1.920	triangle	−1.106	−1.276	−1.060
Surf_1	+0.226	linear	−0.655	−0.872	−1.046

the unit cell in a singlet (zero unpaired electron), triplet (two unpaired electrons), or quintet (four unpaired electrons) state.

We expected that the spin states would play some roles in hydrogen desorption. We calculated the hydrogen desorption energies from various positions of the $TiB_2H_8-nBH_4$ complex structures. We considered the products in different spin states and listed the desorption energies accordingly in Table 2. The numbering of hydrogen atoms in Table 2 was labeled in the local structures shown in Figure 2. For clarity, the lower-energy and, therefore, favorable product states are given in bold. We stress that all of our calculations have been done with the periodic boundary condition using the VASP program. The cluster structures were used for clarity in the presentations. Following the convention that we developed in treating the $TiAl_3H_{12}$ complex, the hydrogen atoms were classified into outside hydrogen atoms ($H_5 \sim H_8$), inside hydrogen atoms ($H_9 \sim H_{12}$), and mixed hydrogen atoms ($H_1 \sim H_4$), according to their relative positions to Ti. As a reference, the hydrogen desorption energies from the undoped (001), (100), and (010) surfaces were calculated as 3.676, 3.856, and 3.768 eV, respectively, and all led to a singlet product state.[32] In general, all hydrogen desorption energies listed in Table 2 are significantly lower than those of the corresponding clean surfaces. The lower desorption energies may favor a quick release of hydrogen from the system, which is consistent with the experimental observation.[11] We believe that the doped Ti in $LiBH_4$ can improve the thermodynamics by reducing dehydrogenation energies and may enhance the dehydriding and rehydriding kinetics through the complex active centers. Although the activation barrier of the elementary step provides some kinetics information about the process, an overall kinetic description needs all of the steps involved in the complicated network of reactions. These steps include hydrogen recombination and desorption as well as hydrogen migration and phase transition. This is beyond the scope of the present paper.

We used S, T, and Q to denote the singlet, triplet, and quintet states, respectively, and summarized possible reactions involved in dehydrogenation into the following reactions:

$$S \rightarrow S + H_2 \quad \text{(R1)}$$

$$S \rightarrow S + H + H \rightarrow S + H_2 \quad \text{(R2)}$$

$$T \rightarrow T + H_2 \quad \text{(R3)}$$

$$T \rightarrow S + H + H \rightarrow S + H_2 \quad \text{(R4)}$$

$$Q \rightarrow Q + H_2 \quad \text{(R5)}$$

$$Q \rightarrow T + H + H \rightarrow T + H_2 \quad \text{(R6)}$$

Reactions R1, R3, and R5 represent one-step pathways for forming a hydrogen molecule, while eqs R2, R4, and R6 are two-step pathways which involve desorbing atomic hydrogen first and recombining the desorbed hydrogen atoms in the gas phase. Along the two-step pathways, the spin state may change as the reaction progresses. For example, triplet $TiB_2H_8-BH_4$ on the (001) surface and $TiB_2H_8-2BH_4$ on the (010) surface can form a singlet product following the H atom desorption, R4, whereas the quintet $TiB_2H_8-BH_4$ on the (100) surface can lead to a triplet product, R6. The desorption energies listed in Table 2 are the overall reaction energies of R3−R6. A triplet product state is energetically more favorable than the singlet product state in the Ti-doped $LiBH_4$ (001) surface. Therefore, we expect that the dehydrogenation of triplet $TiB_2H_8-BH_4$ on the (001) surface will follow the one-step mechanism described in reaction R3 and desorb a hydrogen molecule from the Ti catalytic center. As shown in Table 2, the inside hydrogen atoms (H9−H12) have a much higher desorption energy than those from other positions but are still lower than that of the undoped clean surface. As discussed later, the structural stability really depends on the orbital overlap between inside B−H bonds and Ti. Desorption of inside hydrogen atoms results in a relatively higher desorption energy due to the reduced orbital overlap between Ti and inside B−H bonds.

In contrast, from the quintet $TiB_2H_8-BH_4$ of the Ti-doped $LiBH_4$ (100) surface, the triplet product state upon desorbing hydrogen is favored. Therefore, the quintet $TiB_2H_8-BH_4$ on surface (100) may have a two-step dehydrogenation mechanism, described in reaction R6. Hydrogen atoms are first released from the $TiB_2H_8-BH_4$ cluster and then combine to form a hydrogen molecule in the gas phase. An exception is that some inside hydrogen pairs such as H10−H11 and H10−H12 show much lower desorption energies than the corresponding pairs in the Ti-doped $LiBH_4$ (001) surface. A careful examination revealed that hydrogen desorption from these positions of $TiB_2H_8-BH_4$ in the (100) surface led to outside hydrogen atoms being transferred to inside positions. In contrast, a similar hydrogen transfer was not found in the triplet $TiB_2H_8-BH_4$ in the (001) surface.

For the triplet $TiB_2H_8-2BH_4$ of the Ti-doped $LiBH_4$ (010) surface, the majority of hydrogen desorption pathways still led to triplet states. Desorption of H1−H2, H3−H4, and

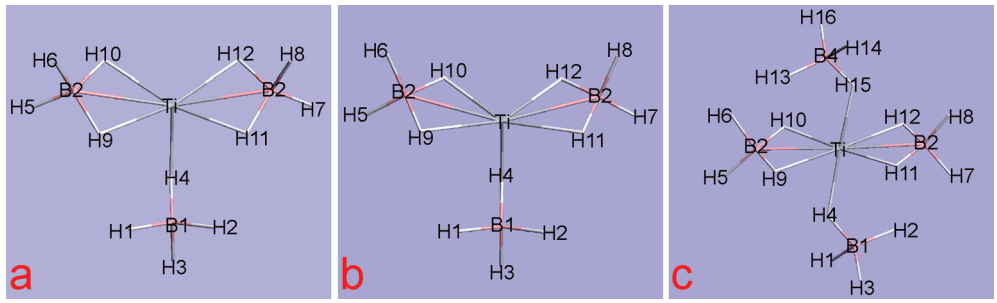

Figure 2. Local structures of the most stable species in the Ti-doped (a) $LiBH_4$(001), (b) $LiBH_4$ (100), and (c) $LiBH_4$ (010).

Table 2. Hydrogen Desorption Energies (unit: eV) of the Most Stable Species in Ti-Doped $LiBH_4$ (001), (100), and (010) Surfaces

	triplet $TiB_2H_8-BH_4$ (001)		quintet $TiB_2H_8-BH_4$ (100)		triplet TiB_2H_8-$2BH_4$ (010)	
	singlet	triplet	triplet	quintet	singlet	triplet
H1−H2	1.092	**0.915**	**−0.028**	1.749	**0.210**	0.389
H3−H4	N/A	**1.193**	**0.587**	1.664	**0.150**	0.387
H5−H6	2.477	**2.312**	**0.698**	1.896	0.473	**0.403**
H5−H7	1.363	**1.070**	**0.463**	2.520	0.550	**0.459**
H6−H7	1.217	**1.095**	**0.513**	2.246	0.759	**0.718**
H6−H8	1.219	**1.088**	**0.557**	2.790	**0.185**	0.221
H9−H10	N/A	N/A	N/A	2.324	0.568	**0.480**
H9−H11	1.510	**1.269**	**2.089**	2.532	0.594	**0.527**
H10−H11	2.101	**1.901**	**0.551**	2.079	0.859	**0.718**
H10−H12	**2.182**	2.248	**0.528**	2.182	0.431	**0.320**

H6−H8 resulted in singlet states. We consider the singlet and triplet states as the competitive hydrogen desorption pathways due to the very similar desorption energies. We would point out that the triplet $TiB_2H_8-2BH_4$ in the (010) surface has lower desorption energies than the triplet and quintet $TiB_2H_8-BH_4$ in the (001) and (100) surfaces, respectively.

3.3. Comparison of Ti-Doped $LiBH_4$ with Ti-Doped $NaAlH_4$. As we stated in the Introduction, the improvement by adding Ti compounds in $LiBH_4$ is not as efficient as doping Ti compounds in $NaAlH_4$.[9,10] A comparison of Ti-doped $LiBH_4$ and Ti-doped $NaAlH_4$ will help to understand the changes that Ti induces in B−H interactions and how these changes affect subsequent dehydriding/rehydriding reactions. Our previous studies of Ti-doped $NaAlH_4$ showed that doped Ti prefers to occupy the interstitial site and interacts with surrounding AlH_4^-, forming a $TiAl_3H_{12}$ species.[14,15] We further suggested the role of the $TiAl_3H_{12}$ complex in dehydriding and hydriding sodium alanate-based hydrogen storage materials.[17]

First of all, our results indicate that Ti energetically prefers to occupy the interstitial positions in both $NaAlH_4$ and $LiBH_4$ surfaces, although the detailed structures of the local complexes in $LiBH_4$ are different from that of Ti-doped $NaAlH_4$. We used $TiB_2H_8-nBH_4$ to represent the complex structures formed from doping Ti in $LiBH_4$. The stability of these species may play an important role in their reactivity for the dehydriding/hydriding reactions. On the other hand, hydrogen desorption energies in both Ti-doped $LiBH_4$ and $NaAlH_4$ were also reduced significantly with respect to that from their corresponding undoped clean surfaces. Dehydriding the $TiB_2H_8-nBH_4$ ($n = 1-2$) species would lead to the formation of TiB_n ($n = 2-3$), which is consistent with the experimental observation.[10]

There are also distinctive discrepancies between Ti-doped $NaAlH_4$ and Ti-doped $LiBH_4$. First, the bond activation by Ti in $LiBH_4$ is much less dramatic than that in $NaAlH_4$. In Ti-doped $LiBH_4$, the inside B−H bonds were only slightly elongated (about 0.02−0.04 Å) compared with the B−H bond in the clean surface. In contrast, two inside A−H bonds in $TiAl_3H_{12}$ of Ti-doped $NaAlH_4$ surfaces were broken, and the dissociated H atoms were transferred to Ti.[14,15] To understand the electronic origin of the difference, we analyzed the densities of state (DOSs) of the most stable interstitial structures (*Inter_1*) on each Ti-doped $LiBH_4$ surface. The DOSs of $TiB_2H_8-BH_4$ in the (001) surface, $TiB_2H_8-BH_4$ in the (100) surface, and TiB_2H_8-$2BH_4$ in the (010) surface were plotted in Figure 3a−c. In each DOS plot, we included the Ti atom, the boron atoms (B1 and B2) of the neighboring BH_4^- units, and the hydrogen atoms (H4, H9, and H10) connected with Ti. The bond-activation difference can be attributed to the back-donation of electrons from the d orbitals of Ti to antibonding orbitals of the B−H bond. In the previous analysis of Ti-doped $NaAlH_4$, we attributed some new peaks at −2 to 0 eV in Al1- and Al2-DOS to electron backdonation from Ti d orbitals to A−H antibonding orbitals.[17] However, similar electron backdonation was not found in the Ti-doped $LiBH_4$ surfaces, although electron donation from bonding orbitals of B−H to the empty orbital of Ti occurred, as shown in low-energy regions (−8∼−6 eV) of Ti-DOS. A lack of backdonation in Ti-doped $LiBH_4$ may be due to the considerable gap between the occupied orbital of Ti and virtual orbitals of BH_4^-. We have demonstrated that the electron back-donation played a dominant role in H−H and A−H bond activation in transition-metal-catalyzed $NaAlH_4$.[17] In the case of Ti-doped $LiBH_4$, the weak backdonation is the main reason for the observed low reactivity.[9,10] Fe and Mo, which have a

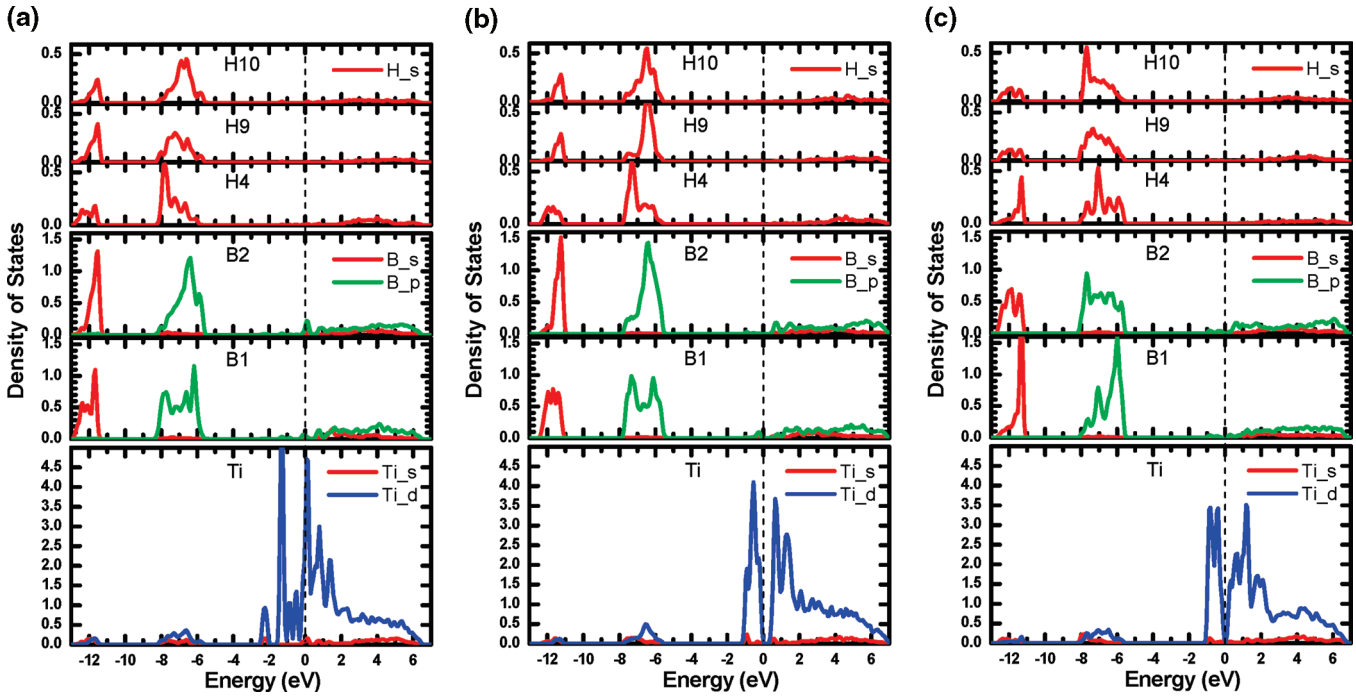

Figure 3. Local densities of state (DOSs) of the H, B, and Ti atoms in the most stable structures, that is, triplet $TiB_2H_8-BH_4$ in the (001) surface, quintet $TiB_2H_8-BH_4$ in the (100) surface, and triplet TiB_2H_8-$2BH_4$ in the (010) surface.

stronger backdonation capability from their occupied orbitals to the virtual orbitals of BH_4^-, may be better catalysts to activate the B−H bonds.[47,48]

Another difference in the two systems lies in the correlation of stability of local structures with the 18-electron rule. The XH_4^- (X = B, Al) ligands can act as a two-, four-, and six-electron donor by coordination of Ti through one, two, or three X−H bonds.[17,19,20,49] Usually, the stability of relaxed structures can be simply predicted by applying the electron-counting rule.[50,51] The total number of electrons surrounding Ti can be calculated by adding its valence electrons and the electrons shared with the ligands. For Ti, 18 electrons are needed to fill the five d orbitals, one s orbital, and three p orbitals in order to reach a closed-shell configuration. In some cases, the complex in a high-spin state accommodates fewer electrons. For example, a 16-electron complex in a triplet state is the most stable. Deviation from this number resulted in less stable structures and, therefore, lower binding energies.[18,19] Unfortunately, the stability order of relaxed structures in the Ti-doped $LiBH_4$ (001) surface does not follow this electron-counting rule. There are a total of 14 electrons surrounding the Ti atom in the most stable structure *Inter_1* of the (001) surface. However, the triplet state is the lower-energy spin-state for *Inter_1*. Similarly, both *Inter_3* and *Inter_4* in the (001) surface have 16 electrons and are in the quintet state instead of the triplet state. Therefore, the electron-counting rule is not strictly applicable in predicting the structural stability of Ti-doped $LiBH_4$. However, in the TM-doped $NaAlH_4$, the stability of most structures was found to follow the 18-electron rule.[17] The difference between Ti-doped $LiBH_4$ and $NaAlH_4$ could be understood by comparing the DOSs of the two systems. In the Ti-doped $NaAlH_4$, there is a very small gap (about 1.5 eV) from the bonding orbitals of Al−H to the d orbitals of Ti. Electrons in these orbitals can be shared, thereby satisfying the closed-shell requirement. On the other hand, there is about a 4 eV gap between the bonding orbitals of B−H and the d orbitals of Ti, as shown in the DOS figures of the Ti-doped $LiBH_4$ surfaces. The large gap makes the electrons in the B−H bond less available to the empty d orbitals of Ti.

We explored further the relationship of stability with the coordination modes of the local structures. First of all, we focus on a linear TiB_2H_8 structure (*Inter_2*) with a double η^2 coordinate mode. Figure 4 shows schematically the molecular orbital overlap between two BH_4^- ligands and the central Ti atom. We did not display the low-energy orbitals formed by the B s orbital and the four remaining H s ones because they were localized mainly on the ligands and interact poorly with transition metals. We only showed the overlaps between Ti d orbitals and ligand orbitals constructed by B p and H s. Under D_{2h} symmetry, two BH_4^- units generate three types of orbitals with the symmetry b_{1g}, b_{2u}, and b_{3u}. According to the orbital symmetry-adapting rule, the ligand orbitals with the symmetries of b_{2u} and b_{3u} only interact poorly with Ti 4s or 4p orbitals. Therefore, the ligand orbitals of b_{2u} and b_{3u} contribute little to the stability of TiB_2H_8. Although symmetrically allowed, the molecular orbital HOMO−1 that is constructed by the Ti d orbital and "outside" B−H bonding orbitals only shows a weak overlap. On the other hand, the molecular orbital HOMO−5 exhibits a significant orbital overlap between Ti d_{xz} and "inside" B−H bonding orbitals. Such an orbital overlap contributes significantly to the stability of the structure.

Another linear TiB_2H_8 structure, *Inter_4* in Ti-doped $LiBH_4$ (001), has a double η^3 coordination mode with a smaller binding energy (−1.581 eV) than that of *Inter_2* (double η^2, −2.409 eV). We also displayed its molecular orbitals, showing the interaction between Ti and two ligands in Figure 4. Under D_{3h} symmetry, two BH_4^- units generate

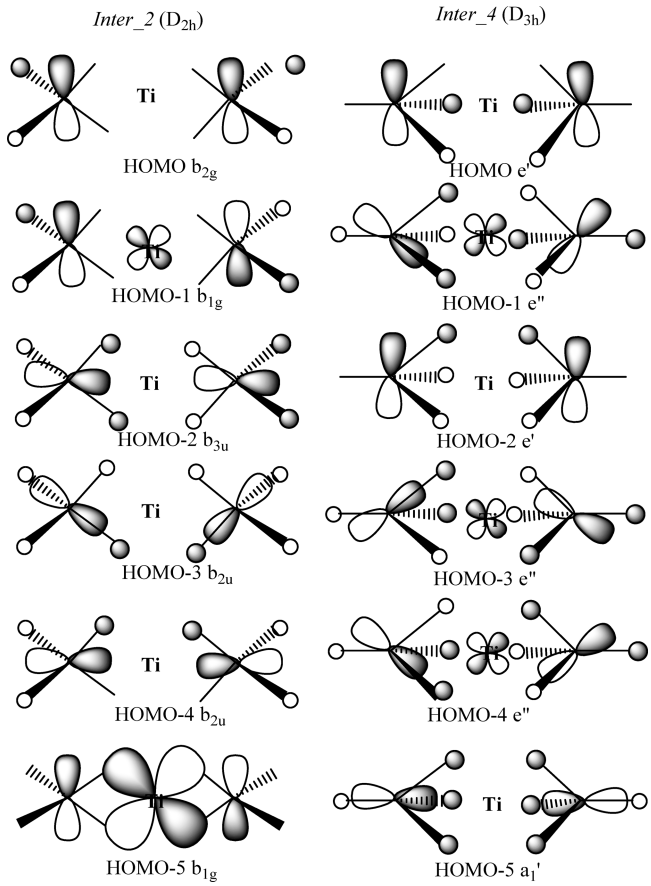

Figure 4. Schematic frontier molecular orbitals of TiB_2H_8 in *Inter_2* and *Inter_4* of Ti-doped $LiBH_4$(001). *Inter_2* and *Inter_4* have a double η^2 coordinate with D_{2h} symmetry and a double η^3 coordinate with D_{3h} symmetry, respectively.

three types of orbitals with the symmetries a_1', e', and e''. However, we expect the ligand orbitals with symmetries a_1' and e' not to make a major contribution to the structural stability. Only e'' orbitals generated by the two ligands are able to overlap with π-type orbitals of Ti. These orbital overlaps are very small because the ligand orbitals are not symmetric and some of the electrons are distributed in the terminal atoms. Therefore, the calculated binding energies of *Inter_4* are much smaller than that of *Inter_2*. For the isolated complexes such as $Ti(BH_4)_3$, ab initio calculations have shown that η^2 and η^3 structures are not much different in binding energy for some transition metals.[23,52−55] Obviously, there is a large difference of stability related to η^2 and η^3 ligands between the isolated complexes $Ti(BH_4)_3$ and $TiB_2H_8-nBH_4^-$ in a solid-state environment.

Finally, $TiB_2H_8-nBH_4$ (n = 1,2) in Ti-doped $LiBH_4$ surfaces is isolated from neighboring BH_4^- units. This is in direct contrast with the $TiAl_3H_{12}$ structure formed in Ti-doped $NaAlH_4$ which links to the neighboring AlH_4^- units and facilitates hydrogen desorption and transfer.[15] This structure difference may offer an explanation for the different amounts of added Ti in $NaAlH_4$ and $LiBH_4$. Experimentally, only ~4 mol % $TiCl_3$ was needed for $NaAlH_4$,[38,43,56−58] whereas 25 mol % $TiCl_3$ or TiO_2 was required to achieve significant reduction in the hydrogen desorption temperature for $LiBH_4$.[9,10]

4. Conclusions

In the present paper, we have studied the energetics and structures of Ti-doped $LiBH_4$ (001), (100), and (010) surfaces using DFT-PBE methods with the plane-wave basis set and PAW potential. On the basis of our results and analysis, we conclude the following:

(1) Ti prefers occupying the interstitial positions among three or four BH_4^- hydrides, forming local complex structures of $TiB_2H_8-nBH_4$ (n = 1, 2) with the high-spin states. The stability of these structures can be explained by orbital overlap between Ti and "inside" B−H bonds.

(2) The desorption energies from many positions of these stable complex structures are reduced significantly with respect to those from the clean surface. The triplet $TiB_2H_8-BH_4$ in (001) and $TiB_2H_8-2BH_4$ in (010) can desorb hydrogen in the form of a H_2 molecule, while the quintet $TiB_2H_8-BH_4$ in (100) preferably desorbs atomic hydrogen.

(3) A comparison between Ti interaction with B−H and A−H revealed that the low reactivity of Ti-doped $LiBH_4$ is a result of the weak back-donation from d orbitals of Ti to the antibonding orbitals of BH_4^-.

Acknowledgment. This work was supported by U.S. Department of Energy, Basic Energy Science grant DE-FG02-05ER46231.

References

(1) Seayad, A. M.; Antonelli, D. M. *Adv. Mater.* **2004**, *16*, 765.

(2) Schlapbach, L.; Züttel, A. *Nature* **2001**, *414*, 353.

(3) Orimo, S.; Nakamura, Y.; Eliseo, J. R.; Züttela, A.; Jensen, C. M. *Chem. Rev.* **2007**, *107*, 4111.

(4) Fedneva, E. M.; Alpatova, V. L.; Mikheeva, V. I. *Russ. J. Inorg. Chem.* **1964**, *9*, 826.

(5) Lide, D. R. *CRC Handbook of Chemistry and Physics*; CRC Press: Boca Raton, FL, 2004; Vol. 84.

(6) Züttel, A.; Rentsch, S.; Fischer, P.; Wenger, P.; Sudan, P.; Mauron, P.; Emmenegger, C. *J. Alloys Compd.* **2003**, *356−357*, 515.

(7) Orimo, S.; Nakamori, Y.; Züttel, A. *Mater. Sci. Eng.* **2004**, *B108*, 51.

(8) Vajo, J. V.; Skeith, S. L.; Mertens, F. *J. Phys. Chem. B* **2005**, *109*, 3719.

(9) Au, M.; Jurgensen, A.; Zeigler, K. *J. Phys. Chem. B* **2006**, *110*, 26482.

(10) Au, M.; Jurgensen, A. *J. Phys. Chem. B* **2006**, *110*, 7062.

(11) Fang, Z. Z.; Ma, L. P.; Kang, X. D.; Wang, P. J.; Wang, P.; Cheng, H. M. *Appl. Phys. Lett.* **2009**, *94*, 044104.

(12) Kelkar, T.; Pal, S. *J. Mater. Chem.* **2009**, *19*, 4348.

(13) Kelkar, T.; Pal, S.; Kanhere, D. G. *ChemPhysChem* **2008**, *9*, 928.

(14) Liu, J.; Ge, Q. *Chem. Commun.* **2006**, 1822.

(15) Liu, J.; Ge, Q. *J. Phys. Chem. B* **2006**, *110*, 25863.

(16) Balde, C. P.; Stil, H. A.; van der Ederden, A. M. J.; de Jong, K. P.; Bitter, J. H. *J. Phys. Chem. B.* **2007**, *111*, 2797.

(17) Liu, J.; Han, Y.; Ge, Q. *Chem.—Eur. J.* **2009**, *15*, 1685.

(18) Volatron, F.; Duran, M.; Lledos, A.; Jean, Y. *Inorg. Chem.* **1993**, *32*, 951.

(19) Lledos, A.; Duran, M.; Jean, Y.; Volatron, F. *Inorg. Chem.* **1991**, *30*, 4440.

(20) Dain, C. J.; Downs, A. J.; Goode, M. J.; Evans, D. G.; Nicholls, K. T.; Rankin, D. W. H.; Robertson, H. E. *J. Chem. Soc., Dalton Trans.* **1991**, *4*, 967.

(21) Hitchkock, A. P.; Hao, N.; Werstiuk, N. H.; Mcglinchey, M. J.; Ziegler, T. *Inorg. Chem.* **1982**, *21*, 793.

(22) Mancini, M.; Bougeard, P.; Burns, R. C.; Mlekuz, M.; Sayer, B. G.; Thompson, J. I. A.; Mcglinchey, M. J. *Inorg. Chem.* **1984**, *23*, 1072.

(23) Jarid, A.; Lledos, A.; Jean, Y.; Volatron, F. *Inorg. Chem.* **1993**, *32*, 4695.

(24) Íñiguez, J.; Yildirim, T.; Udovic, T. J.; Sulic, M.; Jensen, C. M. *Phys. Rev. B* **2004**, *70*, 060701(R).

(25) Kresse, G.; Furthmiiller, J. *Comput. Mater. Sci.* **1996**, *6*, 15.

(26) Kresse, G.; Furthmü ller, J. *Phys. Rev. B* **1996**, *54*, 11169.

(27) Kresse, G.; Joubert, D. *Phys. Rev. B* **1999**, *70*, 1758.

(28) Perdew, J. P.; Burke, K.; Ernzerhof, M. *Phys. Rev. Lett.* **1996**, *77*, 3865.

(29) Perdew, J. P.; Burke, K.; Wang, Y. *Phys. Rev. B: Condens. Matter* **1996**, *54*, 16533.

(30) Monkhorst, H. J.; Pack, J. D. *Phys. Rev. B* **1976**, *13*, 5188.

(31) Liu, J.; Ge, Q. *J. Alloys Compd.* **2007**, *446−447*, 267.

(32) Ge, Q. *J. Phys. Chem. A.* **2004**, *108*, 8682.

(33) Philipsen, P. H. T.; Baerends, E. J. *Phys. Rev. B* **1996**, *54*, 5326.

(34) Frisch, M. J.; Trucks, G. W.; Schlegel, H. B.; Scuseria, G. E.; Robb, M. A.; Cheeseman, J. R.; Montgomery, J. A., Jr.; Vreven, T. K. K. N.; Burant, J. C.; Millam, J. M.; Iyengar, S. S.; Tomasi, J.; Barone, V.; Mennucci, B.; Cossi, M.; Scalmani, G.; Rega, N.; Petersson, G. A.; Nakatsuji, H.; Hada, M.; Ehara, M.; Toyota, K.; Fukuda, R.; Hasegawa, J.; Ishida, M.; Nakajima, T.; Honda, Y.; Kitao, O.; Nakai, H.; Klene, M.; Li, X.; Knox, J. E.; Hratchian, H. P.; Cross, J. B.; Bakken, V.; Adamo, C.; Jaramillo, J.; Gomperts, R.; Stratmann, R. E.; Yazyev, O.; Austin, A. J.; Cammi, R.; Pomelli, C.; Ochterski, J. W.; Ayala, P. Y.; Morokuma, K.; Voth, G. A.; Salvador, P.; Dannenberg, J. J.; Zakrzewski, V. G.; Dapprich, S.; Daniels, A. D.; Strain, M. C.; Farkas, O.; Malick, D. K.; Rabuck, A. D.; Raghavachari, K.; Foresman, J. B.; Ortiz, J. V.; Cui, Q.; Baboul, A. G.; Clifford, S.; Cioslowski, J.; Stefanov, B. B.; Liu, G.; Liashenko, A.; Piskorz, P.; Komaromi, I.; Martin, R. L.; Fox, D. J.; Keith, T.; Al-Laham, M. A.; Peng, C. Y.; Nanayakkara, A.; Challacombe, M.; Gill, P. M. W.; Johnson, B.; Chen, W.; Wong, M. W.; Gonzalez, C.; Pople, J. A. *Gaussian 03*, revision C. 02; Gaussian, Inc: Wallingford, CT, 2004.

(35) Henkelman, G. A., A.; Jonsson, H. *Comput. Mater. Sci.* **2006**, *36*, 354.

(36) Balema, V. P.; Wiench, J. M.; Dennis, K. W.; Pruski, M. *J. Alloys Compd.* **2001**, *329*, 108.

(37) Sandrock, G.; Gross, K. J.; Thomas, G. *J. Alloys Compd.* **2002**, *339*, 299.

(38) Majzoub, E. H.; Gross, K. J. *J. Alloys Compd.* **2003**, *356−357*, 363.

(39) Bellosta von Colbe, J. M.; Bogdanovic, B.; Felderhoff, M.; Pommerin, A.; Schüth, F. *J. Alloys Compd.* **2004**, *370*, 104.

(40) Felderhoff, M.; Klementiev, K.; Grünert, W.; Spliethoff, B.; Tesche, B.; Bellosta von Colbe, J. M.; Bogdanovic, B.; Härtel, M.; Pommerin, A.; Schüth, F.; Weidenthaler, C. *Phys. Chem. Chem. Phys.* **2004**, *6*, 4369.

(41) Graetz, J.; Reilly, J. J.; Johnson, J.; Ignatov, A. Y.; Tyson, T. A. *Appl. Phys. Lett.* **2004**, *85*, 500.

(42) Leon, A.; Kircher, O.; Rothe, J.; Fichtner, M. *J. Phys. Chem. B.* **2004**, *108*, 16372.

(43) Bogdanovic, B.; Schwickardi, M. *J. Alloys Compd.* **1997**, *253−254*, 1.

(44) Streukens, G.; Bogdanovic, B.; Felderhoff, M.; Schuth, F. *Phys. Chem. Chem. Phys.* **2006**, *8*, 2889.

(45) Bogdanovic, B.; Felderhoff, M.; Germann, M.; Hartel, M.; Pommerin, A.; Schuth, F.; Weidenthaler, C.; Zibrowius, B. *J. Alloys Compd.* **2003**, *350*, 246.

(46) Kircher, O.; Fichtner, M. *J. Alloys Compd.* **2005**, *404−406*, 339.

(47) McNamara, W. F.; Duesler, E. N.; Paine, R. T.; Ortiz, J. V.; Kolle, P.; Noth, H. *Organometallics* **1986**, *5*, 380.

(48) Khasnis, D. V.; Toupet, L.; Dixneuf, P. H. *J. Chem. Soc., Chem. Commun.* **1987**, 230.

(49) Demachy, I.; Volatron, F. *Inorg. Chem.* **1994**, *33*, 3965.

(50) Langmuir, I. *Science* **1921**, *54*, 59.

(51) Mingos, D. M. P. *J. Organomet. Chem.* **2004**, *689*, 4420.

(52) Ariafard, A.; Amini, M. M. *J. Orgamomet. Chem.* **2005**, *690*, 84.

(53) Xu, Z.; Lin, Z. *Inorg. Chem.* **1996**, *35*, 3964.

(54) Musaev, D. G.; Morokuma, K. *Organometallics* **1995**, *14*, 3327.

(55) Goebbert, D. J.; Hernandez, H.; Francisco, J. S.; Wenthold, P. G. *J. Am. Chem. Soc.* **2005**, *127*, 11684.

(56) Bogdanovic, B.; Brand, R. A.; Marjanovic, A.; Schwickardi, M.; Tolle, J. *J. Alloys Compd.* **2000**, *302*, 36.

(57) Gross, K. J.; Guthrie, S.; Takara, S.; Thomas, G. *J. Alloys Compd.* **2000**, *297*, 270.

(58) Gross, K. J.; Majzoub, E. H.; Spangler, S. W. *J. Alloys Compd.* **2003**, *356−357*, 423.

CT900287R